Model Predictive Control for Combustion Timing and Load Control in HCCI Engines

2015-01-0822

Published 04/14/2015

Khashayar Ebrahimi and Charles Koch
Univ of Alberta

CITATION: Ebrahimi, K. and Koch, C., "Model Predictive Control for Combustion Timing and Load Control in HCCI Engines," SAE Technical Paper 2015-01-0822, 2015, doi:10.4271/2015-01-0822.

Abstract

A Model Predictive Control (MPC) strategy for Homogeneous Charge Compression Ignition (HCCI) combustion timing and output work control that takes into account actuator constraints is designed. The MPC is based on the linearized version of a nonlinear Control Oriented Model (COM). The COM for the HCCI engine has combustion timing and engine load as outputs and valve timing and fueling rate as the inputs. The COM model is developed and validated and found to be accurate enough for control purposes and can be implemented in real-time. A Detailed Physical Model (DPM) is used to test the controller using the valve timing and fueling rate as constrained actuators. Constraints on combustion timing and output work are also considered to prevent ringing or misfire. The simulation results show that the developed controller works over a range of load conditions and can maintain HCCI combustion timing and load to their desired values.

Introduction

Homogenous Charge Compression Ignition (HCCI) is a promising engine concept that has potential for low emissions while keeping fuel efficiency high [1, 2, 3]. In HCCI engines, a homogeneous air fuel mixture is compressed to the point that combustion starts. Because of the low temperature combustion in HCCI engines, the NO_X level is low, however unburnt HydroCarbons (HC) and CO levels are high [1]. HCCI has an operating range limited by misfire at low loads and ringing at high loads. In addition, HCCI combustion timing is difficult to control compared to other conventional engines such as SI and Diesel, since there is no direct initiator of combustion in HCCI engines [1]. Combustion timing in HCCI engines is influenced by trapped mixture temperature, pressure and composition at Intake Valve Closing (IVC) and in-cylinder mixture homogeneity [4]. The combustion timing in HCCI engines can be controlled by a variety of method such as: adjusting the intake charge temperature [5, 6]; retaining or reinducting hot residual gas from the previous cycle with Variable Valve Timing (VVT) [7, 8, 9, 10, 11, 12, 13]; external Exhaust Gas Recirculation (EGR) [14, 15]; varying the auto-ignition properties of the fuel using dual-fuels [16, 17, 18, 19]; changing the compression ratio [20, 21]; pilot injection [22, 23] and water injection [24, 25]. Intake air heating is not practical because energy is required to heat the air and the heater response time is slow compared to an engine cycle. Exhaust Gas Recirculation (EGR) is usually not fast enough for cycle-by-cycle combustion timing control. Controlling the combustion timing by varying the auto-ignition properties of the fuel using dual-fuels is also effective but at least two fuels are needed. A variable compression ratio engine can also be used to control the combustion timing but requires a complex mechanism. Pilot injection is another interesting technique for combustion timing control, however this technique increases CO and HC emissions and decreases fuel efficiency [26]. Water injection slows down the combustion rate and retards the combustion timing, however, it increases the unburnt HC and CO emissions [24]. With VVT, fast cycle-by-cycle control response can be achieved by changing the amount of trapped residual gas and the effective compression ratio cycle by cycle. Variable valve timing with symmetric Negative Valve Overlap (NVO) strategy is used for cycle-by-cycle combustion timing control in this work. In this strategy, the Exhaust Valves Close (EVC) timing is set before piston reaching the Top Dead Center (TDC) in the exhaust stroke and the Intake Valves Open (IVO) timing is set to the same amount, or symmetric, after TDC (see Figure 1). With symmetric changes of EVC and IVO timing around TDC, the recompression work can be regained as expansion work and the pumping work is minimized with this strategy. The effects of symmetric NVO on HCCI combustion have been investigated in [27, 28, 29, 30, 31]. A typical pressure time history of HCCI engine with symmetric NVO is shown in Figure 2.

Since the ability to control HCCI combustion timing is essential for this type of combustion to be practical in a real engine, a variety of controllers with various complexities have been developed. Some of the controllers are based on models obtained from system identification [10, 33] and many are based on physical models [19, 23, 31, 34].

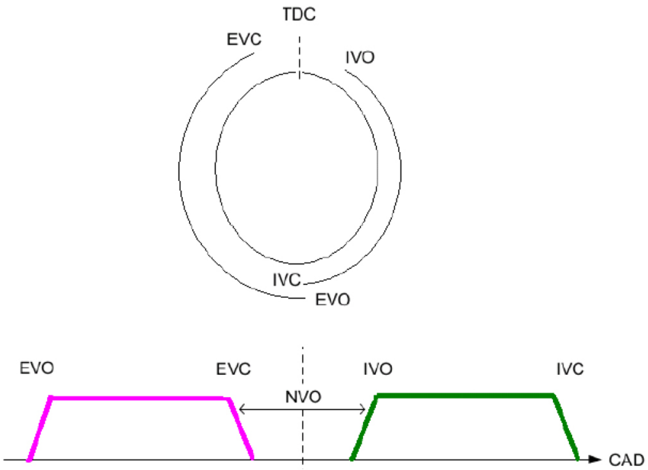

Figure 1. Symmetric negative valve overlap strategy

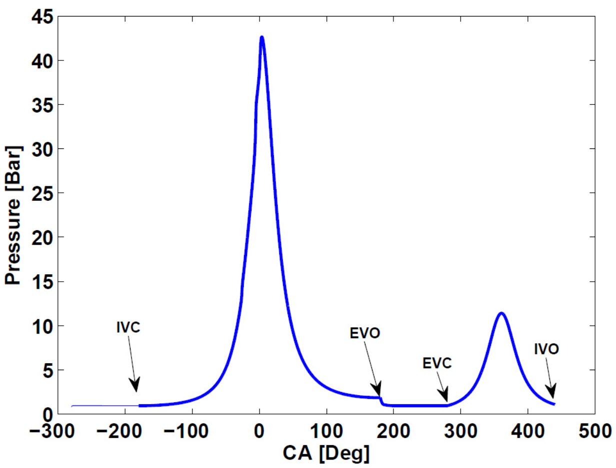

Figure 2. HCCI engine pressure trace with 160 CA Deg NVO duration - obtained from DPM [32]

A short summary of some HCCI combustion timing control is given next to provide context for the control developed in this work. In [35], closed-loop control of the combustion timing and load is performed in an HCCI engine using a gain-scheduled experimentally tuned PID controller with fueling rate and fuel Octane Number (ON) as actuators. A PID controller is developed to vary the ratio of hot to cold intake air entering a variable compression ratio engine in [36] for combustion timing control while fueling rate is used for load control. Compression ratio is varied to control combustion timing and load with a PID controller in [20] and it is tested on a single cylinder research engine. A feedforward controller is developed in [37] based on a physical mean value model to control combustion duration. Combustion duration is controlled by changing the mixing ratios of the cold and hot fresh charge in the intake manifold [37]. In [38], a mean value model is developed using re-breathing technique for combustion timing control in an HCCI engine equipped with variable valve timing. The model has five continuous states which are: intake and exhaust manifold mass and mixture composition and exhaust manifold pressure. The discontinuous states of the model are in-cylinder temperature and pressure at IVC, in-cylinder mixture composition and combustion timing. A LQG controller is described and implemented on a multi-cylinder engine for combustion timing control based on system identification model [39] with fuel ON as main actuator. In [40], a two-input two-output H_2 controller is designed based on a two-state model for combustion timing and peak in-cylinder pressure control. The actuators are EVC and IVC timings and the controller is implemented on a single cylinder research engine. A PID controller is developed and implemented in [12] for combustion timing control where the actuators are EVC and IVO timings. Cylinder to cylinder cross talk in a multi cylinder HCCI engine is modeled in [41] and a LQG controller is used to control combustion timing for each cylinder. In [9], a layered closed loop control for an HCCI engine equipped with variable valve timing is implemented by combining classical PID and a feed forward control strategy to realize effective control of load and combustion timing. A feedforward-feedback controller is developed in [42] for combustion timing and load control. The controller is based on a four-state linear model with oxygen and fuel concentration, temperature and in-cylinder volume at IVC as the states. In [31], a feedforward-feedback controller is developed and implemented in a single cylinder research engine. θ_{50} is used as feedback to the controller and EVC and IVO timings are modulated for combustion timing control. In [43], closed loop control for HCCI combustion timing and load control is developed using adaptative neural network and the actuators are split fuel injection and EVC timing. A PID control strategy for combustion timing control in a single cylinder research engine is described in [44]. Combustion timing is used as feedback to the controller and a hybrid hardware-software system is used for combustion timing measurement. NVO duration and IVC timing are used as two different actuators for combustion timing control [44]. In [19], a Discrete Sliding Mode Controller (DSMC) coupled with a Kalman filter is designed to control combustion timing by adjusting the ratio of two Primary Reference Fuels (PRFs) while a feed-forward controller is used for load control [45]. The controller is designed based on a five-state model. The model states are θ_{50}, temperature and pressure at start of combustion and residual gas mass fraction and temperature. The model developed in [45] is used for combustion timing and load control in [46] with fuel ON and fuel equivalence ratio as actuators. The desired combustion timing trajectory is calculated from experimental desired load trajectory and an integral state feedback controller is used for combustion timing control while a feedforward controller is used for load control. The control oriented model used in [19, 45, 46] is developed based on extensive experimental data and is not easy to apply for engines with different configuration and fuels. MPC is designed in [23] based on a five-state model for combustion timing and output work control with valve timing and split fuel injection as main actuators. The physical model used in [23] is the model developed in [42] with split injection combustion threshold as new state. In [47], MPC is designed based on the model developed in [23] for combustion timing and load control while maintaining the equivalence ratio within an acceptable range. The controller is tested on a multi-cylinder HCCI engine with the same actuators used in [23]. In [48], MPC is developed based on a model obtained from system identification. The model inputs are IVC timing, intake manifold temperature, engine speed and injected fuel energy. Considering constraints on rate of pressure rise; θ_{50} and IMEP are controlled using IVC timing and fueling rate as main actuators. In [49], MPC is detailed and tested in simulation for maximum in-cylinder pressure and combustion timing control with EVC and IVC timings as main actuators. The controller is based on a four-state physical model with in-cylinder IVC and SOC volumes, residual mole fraction and maximum in-cylinder pressure are the states.

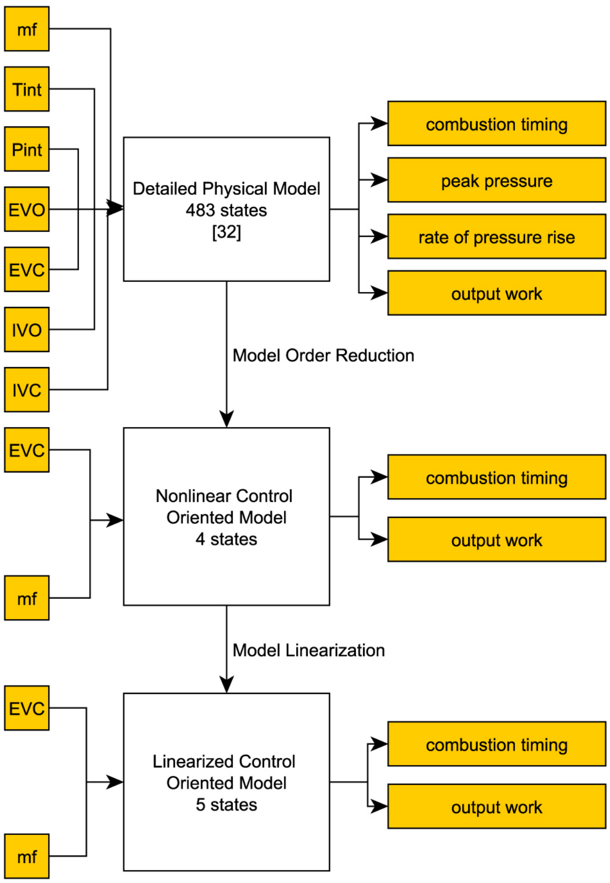

Figure 3. Control Oriented Model development steps

In this study, a 2-step strategy for HCCI combustion model based control is described. First, a nonlinear control oriented model for cycle by cycle combustion timing and output work control is developed. The developed control oriented model is based on model reduction from the detailed physical model developed in [32]. Since the DPM is based on physics and has a Chemical Kinetic Model of the fuel this will allow different fuels and engine configurations to be easily examined if the appropriate fuel chemical kinetics are known. In previous studies [11, 19, 23, 34, 40, 42, 45, 48, 50], either knock integral [51, 52] or Arrhenius type models [40, 53] are used for combustion timing prediction. Such models rely on extensive experimental data for parametrization and they are only valid for limited engine operating ranges. For the case studied here with primary reference fuels, the reaction mechanism is available in [54, 55]. The nonlinear model is then linearized around one operating point and engine experimental validation results show that it has sufficient accuracy for combustion timing and output work prediction. Then symmetric negative valve overlap with variable valve timing is used for HCCI combustion timing control while the fueling rate is used for output work control. The crank angle of fifty percent fuel mass fraction burned, θ_{50}, is used as the cycle by cycle measurement of combustion timing. In simulation, the DPM, presented in [32], provides θ_{50} while in the experiment, cylinder pressure is needed. A schematic of the steps needed to obtain the control oriented model are shown in Figure 3. MPC with Laguerre function are used as the ability to incorporate constraints on inputs and outputs explicitly. This approach is very useful in this highly constrained problem. The Laguerre function is mainly used for the cases when the discrete-time impulse response of a dynamic system is available by a Laguerre model [56]. This approach simplifies the traditional MPC algorithm used in [10, 23, 49, 47] and reduces the computation time [56]. In the next sections, the controller performance is tested with noisy measurement considering constraints on inputs and outputs in simulation. Finally, the controller ability in rejecting engine load and speed disturbances are examined.

Control Oriented Model

A discrete nonlinear control oriented model is developed based on the DPM in [32] and the methods described in [19, 23, 57, 58, 59] for model order reduction. DPM is a crank angle based filling and emptying model. The engine cylinder is modeled as a time variant volume and the cylinder contents are divided into fourteen continuous zones. Conservation of mass is used to obtain set of differential equations for the change in species concentration and energy conservation is used to obtain a differential equation for the temperature change in each zone. Mass transfer between zones is neglected, however, heat transfer is considered. For combustion simulation, a reduced order reaction mechanism for n-heptane [55] is used. The reaction mechanism consists of 29 species and 52 reactions. The in-cylinder pressure is calculated by applying ideal gas law to the cylinder contents. The DPM has 483 states with 7 inputs and 4 outputs. The model inputs are the intake manifold temperature and pressure, fueling rate, IVC, IVO, EVO and EVC timings. The model outputs are combustion timing, maximum rate of pressure rise, maximum in-cylinder pressure and output work. The DPM is detailed in [32].

For the control oriented HCCI engine model, compression, combustion and expansion are modeled as a sequence of continuous processes. The four states of the nonlinear control oriented model are: residual gas mole fraction (α), fuel equivalence ratio (ϕ), in-cylinder temperature at IVC (T_{IVC}) and crank angle of fifty percent fuel mass fraction burned (θ_{50}). These states are found to be important variables affecting HCCI combustion [30, 60]. The control oriented model can be easily modified for other fuels by a model parametrization using the DPM with the appropriate fuel chemical kinetics. Mixture temperature and composition at the beginning of compression are determined first by assuming that the fresh intake charge and residual gas from previous cycle mix instantaneously in the cylinder at IVC. Mixture composition at the beginning of compression is assumed to be:

$$\phi_k C_7H_{16} + 11(O_2 + 3.76N_2) + \alpha_k(7\phi_{k-1}CO_2 \\ + 8\phi_{k-1}H_2O + 41.36N_2 + 11(1-\phi_{k-1})O_2) \tag{1}$$

where ϕ and k represent the fuel equivalence ratio and cycle number respectively. Mixture composition in Equation 1 is determined by assuming that the exhaust gas fuel equivalence ratio is the same as mixture fuel equivalence ratio before combustion [61]. The residual gas mole fraction, α, is calculated as:

$$\alpha_k = \frac{\frac{P_{exh,k-1}V_{EVC,k-1}}{T_{RES,k-1}}}{\frac{P_{int,k}V_{IVC,k}}{T_{IVC,k}}}. \tag{2}$$

Mixture temperature at IVC is determined by using the intake charge composition and applying the first law of thermodynamics to the system. In-cylinder gas temperature at IVC, T_{IVC}, is calculated as:

$$T_{IVC,k} = \frac{C_1 T_{int,k} + \alpha_k C_2 T_{RES,k-1}}{C_1 + \alpha_k C_2} \tag{3}$$

where

$$C_1 = \phi_k C_{p,C_7H_{16}} + 11C_{p,O_2} + 41.36C_{p,N_2}$$
$$C_2 = 7\phi_{k-1}C_{p,CO_2} + 8\phi_{k-1}C_{p,H_2O} + 41.36C_{p,N_2} + 11(1-\phi_{k-1})C_{p,O2}.$$

The specific heat values are assumed to be constant. The in-cylinder pressure at IVC is assumed to be equal to the intake manifold pressure. Temperature and pressure at the crank angle of fifty percent fuel mass fraction burned with the assumption of isentropic compression can then be calculated as

$$T_{50,k} = T_{IVC,k}\left(\frac{V_{IVC,k}}{V_{50,k}}\right)^{\gamma-1} \tag{4}$$

$$P_{50,k} = P_{IVC,k}\left(\frac{V_{IVC,k}}{V_{50,k}}\right)^{\gamma} \tag{5}$$

where Υ is specific heat ratio. Mixture temperature, pressure and composition at IVC are important factors that influencing HCCI combustion timing [1, 30, 60]. To obtain a model that is more suitable for realtime combustion timing control, the DPM is reduced to a fitted algebraic equations for predicting fuel equivalence ratio, start of combustion, combustion duration and crank angle of fifty percent fuel mass fraction burned. The model is:

$$\phi_k = 2.0743T_{RES,k}^{-5.0268} + 0.795m_{fuel,k}Q_{LHV} - 0.0082\alpha_k^{2.4260} + 0.0172. \tag{6}$$

$$\theta_{soc,k} = -0.0047T_{IVC,k} - 0.9479\phi_k + 1.9579 \tag{7}$$

$$\Delta\theta_k = 0.8153\theta_{soc,k} + 0.1925 \tag{8}$$

$$\theta_{50,k} = \theta_{soc,k} + 0.5\Delta\theta_k \tag{9}$$

Constants in equations 6, 7, 8 and 9 are parameterized using the detailed physical model without considering external EGR. Temperature after combustion, T_{AC}, is calculated by applying first law of thermodynamics to the trapped in-cylinder mixture as [34, 49, 58]

$$T_{AC,k} = \frac{(C_1 + \alpha_k C_2)T_{50,k} + C_5}{C_2(1+\alpha_k)} \tag{10}$$

where $C_5 = Q_{LHV\,\phi k}\,\beta$ and β is the percentage of system energy lost by heat transfer during combustion (β=0.12). By applying the ideal gas law to the system, the in-cylinder pressure after combustion, P_{AC} for cycle k is calculated as [34, 49, 58]

$$P_{AC,k} = \frac{N_{AC,k}}{N_{BC,k}}P_{50,k}\frac{T_{AC,k}}{T_{50,k}} \tag{11}$$

where

$$N_{AC,k} = 4\phi_k + 52.36 + \alpha_k(4\phi_{k-1} + 52.36)$$
$$N_{BC,k} = \phi_k + 52.36 + \alpha_k(4\phi_{k-1} + 52.36).$$

The expansion process is assumed to be isentropic so the in-cylinder gas temperature and pressure at EVO is calculated as

$$T_{EVO,k} = (\frac{V_{50,k}}{V_{EVO,k}})^{\gamma-1}T_{AC,k} \tag{12}$$

$$P_{EVO,k} = (\frac{V_{50,k}}{V_{EVO,k}})^{\gamma}P_{AC,k}. \tag{13}$$

At EVO, blowdown to the exhaust manifold pressure is occurred assuming that the in-cylinder mixture isentropically expands to the exhaust manifold pressure. Residual gas temperature after blowdown, T_{RES}, is calculated as [59]

$$T_{RES,k} = \left(\frac{P_{exh,k}}{P_{EVO,k}}\right)^{\frac{\gamma-1}{\gamma}} T_{EVO,k} \tag{14}$$

Finally, engine output work is calculated from a correlation obtained from the DPM:

$$\text{IMEP}_k = 13.7327 \times m_{f,k}Q_{LHV} - 3.887. \tag{15}$$

To write the model in state space form where the states can be written as a function of the inputs and state variables of the previous cycle the model equations are rearranged.

The *first state* equation is residual mole fraction which is given in equation 2. Equations 3, 4, 5, 10, 11, 12, 13 and 14 can then be sequentially substituted into equation 2 to obtain the state equation for the residual mole fraction which is:

$$\alpha_k = \frac{\mathrm{P_{exh}\,T_{int}\,V_{EVC,k-1}}\left(\frac{\mathrm{V_{50,k-1}}}{\mathrm{V_{EVO,k-1}}}\right)^{1-\gamma}}{\mathrm{P_{int}\,V_{IVC}}\left(\mathrm{Q_{LHV}}\,\beta\,\phi_{\mathrm{k-1}} + \mathrm{T_{IVC,k}}\left(\frac{\mathrm{V_{IVC}}}{\mathrm{V_{50,k-1}}}\right)^{\gamma-1} A_2\right)} \times \frac{(\alpha_{\mathrm{k-1}}+1)\;A_1}{A_4^{\frac{\gamma-1}{\gamma}}} \tag{16}$$

where

$$\begin{aligned}
A_1 =&41.36C_{p,N_2} + 7\,\mathrm{C_{p,CO_2}}\,\phi_{\mathrm{k-1}} + 8\,\mathrm{C_{p,H_2O}}\,\phi_{\mathrm{k-1}}\\
&- \mathrm{C_{p,O_2}}\,(11\,\phi_{\mathrm{k-1}} - 11)\\
A_2 =&41.36C_{p,N_2} + 11\,\mathrm{C_{p,O_2}} + \mathrm{C_{p,C_7H_{16}}}\,\phi_{\mathrm{k-1}} + \alpha_{\mathrm{k-1}}\,A_1\\
A_3 =&\mathrm{Q_{LHV}}\,\beta\phi_{\mathrm{k-1}} + \mathrm{T_{IVC,k}}\left(\frac{\mathrm{V_{IVC}}}{\mathrm{V_{50,k-1}}}\right)^{\gamma-1} A_2\\
A_4 =&\left(\frac{\mathrm{P_{exh}}\,\mathrm{T_{IVC,k-1}}\,(\alpha_{\mathrm{k-1}}+1)}{\mathrm{P_{int}}\left(\frac{\mathrm{V_{IVC}}}{\mathrm{V_{50,k-1}}}\right)\left(\frac{\mathrm{V_{50,k-1}}}{\mathrm{V_{EVO,k-1}}}\right)^{\gamma}}\right)\times\\
&\left(\frac{(\phi_{\mathrm{k-1}} + \alpha_{\mathrm{k-1}}\,(4\,\phi_{\mathrm{k-1}} + 41.56) + 41.56)\,A_1}{A_3\,(4\,\phi_{\mathrm{k-1}} + \alpha_{\mathrm{k-1}}\,(4\,\phi_{\mathrm{k-1}} + 41.56) + 41.56)}\right).
\end{aligned}$$

The *second state* equation is the temperature at IVC. Substituting equations 4, 5, 10, 11, 12, 13, 14 and 16 into equation 3 yields the second of these state update equations.

$$T_{IVC,k} = \frac{\left(T_{int}B_{10} - \frac{B_1^{-1}B_4B_{10}B_5}{(\alpha_{k-1}+1)F_3}\right)}{\left(B_{10} + \frac{B_{14}}{P_{int}V_{IVC}B_2B_5}\right)} + B_5 \tag{17}$$

where

$$\begin{aligned}
B_1 =&\left(\frac{V_{50,k-1}}{V_{EVC}}\right)^{1-\gamma}\\
B_2 =&\alpha_{k-1}(4\phi_{k-1} + 52.36)\\
B_3 =&41.36C_{p,N_2} + 7C_{p,CO_2}\phi_{k-1} + 8C_{p,H_2O}\phi_{k-1}\\
&- C_{p,O_2}(11\phi_{k-1} - 11)\\
B_4 =&Q_{LHV}\beta\phi_{k-1} + T_{IVC,k-1}\left(\frac{V_{IVC}}{V_{50,k-1}}\right)^{\gamma-1}\times\\
&(41.36C_{p,N_2} + 11C_{p,O_2} + C_{p,C_7H_{16}}\phi_{k-1} + \alpha_{k-1}B_3)\\
B_5 =&\left(\frac{P_{exh}T_{IVC,k-1}V_{50,k-1}(\alpha_{k-1}+1)}{P_{int}V_{IVC}B_4(4\phi_{k-1} + B_2 + 52.36)\left(\frac{V_{50,k-1}}{V_{EVO}}\right)^{\gamma}}\right)^{\frac{\gamma-1}{\gamma}}\\
&\times((\phi_{k-1} + B_2 + 52.36)\,B_3)^{\frac{\gamma-1}{\gamma}}\\
B_6 =&\frac{B_1^{-1}B_4B_5}{(\alpha_{k-1}+1)B_3}\\
B_7 =&\left(\frac{P_{exh}T_{int}V_{EVC,k-1}B_1(\alpha_{k-1}+1)B_3}{P_{int}V_{IVC}B_4B_5}\right)^{2.426}\\
B_8 =&10000B_6^{5.0268}\\
B_9 =&C_{p,C_7H_{16}}(0.795m_{f,k-1}Q_{LHV} - 0.0082B_7\\
&+ \frac{20743}{B_8} + 0.0172)\\
B_{10} =&41.36C_{p,N_2} + 11C_{p,O_2} + B_9\\
B_{11} =&C_{p,O_2}(8.745m_{f,k-1}Q_{LHV} - 0.0902B_7 + \frac{228173}{B_8}\\
&- 10.8108)\\
B_{12} =&C_{p,CO_2}(5.65m_{f,k-1}Q_{LHV} - 0.0082B_7 + \frac{145201}{B_8}\\
&+ 0.0124) + 41.36C_{p,N_2}\\
B_{13} =&C_{p,H_2O}(6.37m_{f,k-1}Q_{LHV} - 0.0656B_7 + \frac{16.5944}{B_6^{5.0268}}+\\
&0.1376) + B_{12} - B_{11}\\
B_{14} =&P_{exh}T_{int}V_{EVC,k-1}B_1(\alpha_{k-1}+1)B_{13}B_3
\end{aligned}$$

The *third state* equation is fuel equivalence ratio. Similar to the second state update equation, equations 4, 5, 10, 11, 12, 13, 14 and 16 are substituted into equation 6 resulting in:

$$\begin{aligned}
\phi_k =& 0.795\mathrm{m_{f,k-1}Q_{LHV}} + \frac{2.0743}{C_7^{0.5027}} - 0.0082\times\\
&\frac{\left(\mathrm{P_{exh}}\,\mathrm{T_{int}}\,\mathrm{V_{EVC,k-1}}\left(\frac{\mathrm{V_{50,k-1}}}{\mathrm{V_{EVO}}}\right)^{1-\gamma}(\alpha_{\mathrm{k-1}}+1)\,C_1\right)^{2.4}}{C_6}\\
&+ 0.0172
\end{aligned} \tag{18}$$

where

$$\begin{aligned}
C_1 =&41.36\mathrm{C_{p,N2}} + 7\,\mathrm{C_{p,co_2}}\,\phi_{\mathrm{k-1}}\\
&+ 8\,\mathrm{C_{p,H_2O}}\,\phi_{\mathrm{k-1}} - \mathrm{C_{p,O_2}}\,(11\,\phi_{\mathrm{k-1}} - 11)\\
C_2 =&C_1^{\frac{\gamma-1}{\gamma}}(\phi_{\mathrm{k-1}} + \alpha_{\mathrm{k-1}}\,(4\,\phi_{\mathrm{k-1}} + 52.36) + 52.36)^{\frac{\gamma-1}{\gamma}}\\
C_3 =&41.36\mathrm{C_{p,N2}} + 11\,\mathrm{C_{p,O_2}} + \mathrm{C_{p,C_7H_{16}}}\,\phi_{\mathrm{k-1}} + \alpha_{\mathrm{k-1}}\,C_1\\
C_4 =&\mathrm{P_{exh}}\,\mathrm{T_{IVC,k-1}}\,(\frac{\mathrm{V_{IVC}}}{\mathrm{V_{50,k-1}}})^{\gamma-1}(\alpha_{\mathrm{k-1}}+1)\,(\phi_{\mathrm{k-1}}+\\
&\alpha_{\mathrm{k-1}}\,(4\,\phi_{\mathrm{k-1}} + 52.36) + 52.36)\,C_1\\
C_5 =&(4\,\phi_{\mathrm{k-1}} + \alpha_{\mathrm{k-1}}\,(4\,\phi_{\mathrm{k-1}} + 52.36) + 52.36)\mathrm{P_{int}}\,(\frac{\mathrm{V_{IVC}}}{\mathrm{V_{EVO}}})^{\gamma}\\
&\times(\mathrm{Q_{LHV}}\,\beta,\phi_{\mathrm{k-1}} + \mathrm{T_{IVC,k-1}}\,(\frac{\mathrm{V_{IVC}}}{\mathrm{V_{50,k-1}}})^{\gamma-1}\,41.36\mathrm{C_{p,N2}}\\
C_6 =&\mathrm{P_{int}}\,\mathrm{V_{IVC}}\,(\mathrm{Q_{LHV}}\,\beta,\phi_{\mathrm{k-1}} + \mathrm{T_{IVC,k-1}}\,(\frac{\mathrm{V_{IVC}}}{\mathrm{V_{50,k-1}}})^{\gamma-1}\times\\
&C_3)\left(\frac{C_4}{C_5}\right)^{\frac{\gamma-1}{\gamma}}\\
C_7 =&((\alpha_{\mathrm{k-1}}+1)\,C_1)^{-1}(\frac{\mathrm{V_{50,k-1}}}{\mathrm{V_{EVO}}})^{\gamma-1}\times\\
&(\mathrm{Q_{LHV}}\,\beta,\phi_{\mathrm{k-1}} + \mathrm{T_{IVC,k-1}}\,(\frac{\mathrm{V_{IVC}}}{\mathrm{V_{50,k-1}}})^{\gamma-1}\times\\
&(41.36\mathrm{C_{p,N2}} + 11\,\mathrm{C_{p,O_2}} + \mathrm{C_{p,C_7H_{16}}}\,\phi_{\mathrm{k-1}}\\
&+ \alpha_{\mathrm{k-1}}\,C_1))\,C_5{}^{-1}\times\\
&(\mathrm{P_{exh}}\,\mathrm{T_{IVC,k-1}}\,(\frac{\mathrm{V_{IVC}}}{\mathrm{V_{50,k-1}}})^{\gamma-1}(\alpha_{\mathrm{k-1}}+1)\,)^{\frac{\gamma-1}{\gamma}}C_2\\
&+ 11\,\mathrm{C_{p,O_2}} + \mathrm{C_{p,C_7H_{16}}}\,\phi_{\mathrm{k-1}} + \alpha_{\mathrm{k-1}}\,C_1))
\end{aligned}$$

The *fourth state* equation is crank angle of fifty percent fuel mass fraction burned, θ_{50}. Equations 17, 18, 7 and 8 are substituted into equation 9, and the result is:

$$\begin{aligned}
\theta_{50,k} =&0.0109D_9 - 2.7677D_8^{-1} - 1.0607m_{f,k-1}Q_{LHV}\\
&- 0.0066(T_{int}\,(41.36C_{p,N_2} + 11C_{p,O_2} + D_5)\\
&+ \frac{P_{exh}T_{int}V_{EVC,K-1}F_{10}}{P_{int}V_{IVC}})\\
&\times(41.36C_{p,N_2} + 11C_{p,O_2} + D_5 + D_{11})^{-1} + 2.829
\end{aligned} \tag{19}$$

where

$$
\begin{aligned}
D_1 =& \left(\frac{V_{IVC}}{V_{50,k-1}}\right)^{\gamma-1}\\
D_2 =& 41.36C_{p,N_2} + 7C_{p,CO_2}\phi_{k-1}\\
& + 8C_{p,H_2O}\phi_{k-1} - C_{p,O_2}\left(11\phi_{k-1} - 11\right)\\
D_3 =& \left(\frac{V_{50,k-1}}{V_{EVO}}\right)^{1-\gamma}\\
D_4 =& \alpha_{k-1}\left(4\phi_{k-1} + 52.36\right)\\
D_5 =& C_{p,C_7H_{16}}(0.795m_{f,k-1}Q_{LHV}\\
D_6 =& Q_{LHV}\beta\phi_{k-1} + T_{IVC,k-1}D_1\\
& (41.36C_{p,N_2} + 11C_{p,O_2} + C_{p,D_6H_{16}}\phi_{k-1} + \alpha_{k-1}D_2)\\
& + 2.0743D_8^{-1} - 0.0082D_9 + 0.0168)\\
D_7 =& \left(\frac{P_{exh}T_{IVC,k-1}D_1(\alpha_{k-1}+1)(\phi_{k-1}+D_4+52.36)D_2}{P_{int}\left(\frac{V_{IVC}}{V_{EVO}}\right)^{\gamma}D_6(4\phi_{k-1}+D_4+52.36)}\right)^{\frac{\gamma-1}{\gamma}}\\
D_8 =& \frac{\left(\frac{V_{50,k-1}}{V_{EVO}}\right)^{\gamma-1}D_6D_7}{(\alpha_{k-1}+1)D_2}\\
D_9 =& \left(\frac{P_{exh}T_{int}V_{EVC,k-1}D_3(\alpha_{k-1}+1)D_2}{P_{int}V_{IVC}D_7D_6}\right)^{2.426}\\
D_{10} =& 41.36C_{p,N_2} + C_{p,H_2O}(m_{f,k-1}Q_{LHV} + 16.59D_8^{-1}\\
& - 0.0656D_9 + 0.1376) + C_{p,CO_2}(92.75m_{f,k-1}Q_{LHV}\\
& + 14.52D_8^{-1} - 0.0574D_9 + 0.1204)\\
& - C_{p,O_2}(8.75m_{f,k-1}Q_{LHV} + 22.8173D_8^{-1}\\
& - 0.083D_9 - 10.81)\\
D_{11} =& \frac{P_{exh}T_{int}V_{EVC,k-1}D_3(\alpha_{k-1}+1)D_{10}D_2}{P_{int}V_{IVC}D_6D_7}.
\end{aligned}
$$

Equations 16, 17, 18, 19 are now in a form suitable for nonlinear state-space control development. This nonlinear discrete COM can capture the dynamics of trapped residual gas in the HCCI engine cycle by cycle in this form. Figure 4 shows the response of the nonlinear COM to a step change in NVO duration and fueling rate compared with the response of the detailed physical model. A good dynamic match between the nonlinear COM and DPM is observed. Then, the nonlinear COM is linearized around one operating point and the linearized model behavior is compared to both nonlinear COM and detailed physical model in Figure 4. The operating point is selected based on the experimental data in [30] to ensure that the selected point is far away from misfire and ringing regions.

The linear state space model is given by:

$$
\begin{aligned}
x_{k+1} &= Ax_k + Bu_k\\
y_k &= Cx_k + Du_k
\end{aligned}
\tag{20}
$$

where A, B, C and D depend on the operating condition that the model is linearized around. The operating condition that the nonlinear COM was linearized around is listed in Table 1. The model states, inputs and outputs are: $x = [T_{ivc}\ \alpha\ \phi\ m_fQ_{LHV}\ \theta_{50}]^T$, $u = [m_fQ_{LHV}\ \theta_{EVC}]^T$ and $y = [\theta_{50}\ \text{IMEP}]^T$ respectively. m_fQ_{LHV} is added as a new state for the linearized model to make matrix D in equation 20 zero. The A, B and C matrixes of equation 20 are then:

$$
A = \begin{bmatrix} 0.1415 & -4.4917 & 14.79502 & 0 & 1.4264\\ -0.0004 & 0.0144 & -0.0477 & 0 & -0.0046\\ 0.0000 & -0.00002 & 0.00008 & 0 & 0.00000\\ 0 & 0 & 0 & 0 & 0\\ -0.00093 & 0.02975 & -0.09799 & 0 & -0.00944 \end{bmatrix}
$$

$$
B = \begin{bmatrix} 0.2672 & -10.3807\\ 0 & -0.3226\\ 0.795 & 0.0005\\ 1.0000 & 0\\ -1.0625 & 0.0679 \end{bmatrix}
$$

$$
C = \begin{bmatrix} 0 & 0 & 0 & 0 & 1.00\\ 0 & 0 & 0 & 13.732 & 0 \end{bmatrix}
\tag{21}
$$

As seen in equation 21, the fourth state has no dynamics.

Table 1. Operating point for linearization of COM

T_{int}	80^o C
ϕ	0.3
T_{IVC}	86^oC
θ_{EVC}	40 Deg CA bTDC
m_fQ_{LHV}	0.42 kJ
θ_{50}	4.63 Deg CA aTDC
P_{int}	88.6 kPa
ω	820 RPM

Model Validation

Experimental data from the single cylinder engine [30] is compared with the COM and the DPM when NVO duration and fueling rate are varied. In all cases, the charge is lean. First, NVO duration is kept constant and fueling rate is varied. As shown in Figure 5, combustion timing is advanced when fueling rate is increased. The reason is the reactivity of the fuel tends to increase from very lean to richer conditions. Both models show earlier combustion timing as the mixture gets reacher. This is consistent with the literature [30, 60]. Next, the fueling rate is kept constant and NVO duration is changed. Figure 6 shows the effects of NVO duration on combustion timing. When NVO duration increases, the amount of trapped residual gas as well as the in-cylinder gas temperature at IVC increases. Combustion timing is advanced when the in-cylinder gas temperature at IVC increases with larger amounts of internal EGR. This is consistent with the studies [30, 62]. These results confirm that both COM and DPM seem to capture the fueling rate and the trapped residual gas effects on combustion timing. In Figure 7, both COM and DPM models are validated more against 44 engine steady state operating conditions listed in Table 2. These results show that the DPM and COM capture combustion timing with average errors of 1.1 CAD and 1.7 CAD respectively. COM is sufficient for real time requiring 6.4 msec to simulate an HCCI cycle on a 2.66 GHz Intel PC. The DPM requires 22.8 sec for an HCCI cycle which is also relatively fast for this type of simulation.

Figure 8 shows the performance of the DPM, COM and the linearized COM in predicting θ_{50} during transient valve timing experiments. The linear model is compared to the DPM in Figure 9. As shown in this figure, the linear model states track the DPM well. The linear model captures the system dynamics behavior and the maximum error in combustion timing prediction is 1.2 CA Deg compared to the DPM.

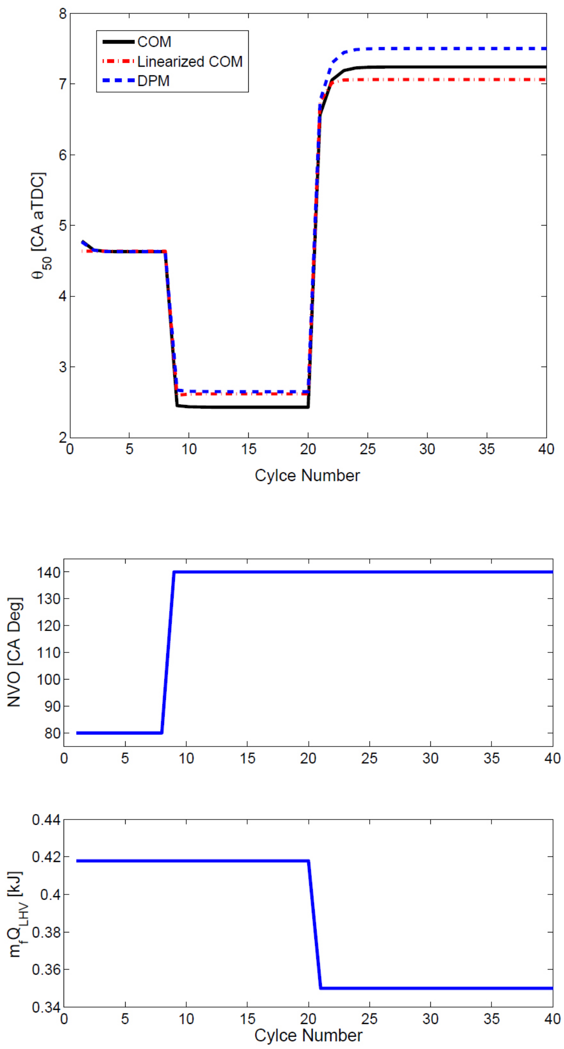

Figure 4. Comparison of the DPM, COM and the linear model for a step change in NVO and then fueling rate

Table 2. Steady state engine operating conditions

T_{int}	78^o - 85^o C
ϕ	0.3 - 0.4
θ_{EVC}	0 - 90 Deg CA bTDC
$m_f Q_{LHV}$	0.33 - 0.49
P_{int}	88 - 95 kPa
ω	813 - 825 RPM
NVO	0 - 180 CA Deg

The linearized COM is used for MPC [56] design considering constraints on inputs and outputs. θ_{50} and engine output work are used as controller inputs and the outputs are NVO duration and fueling rate. Constraints on θ_{50} and output work are sufficient for safe engine operation mode. Constraints on NVO duration and fueling rate are determined based on the experimental limits. The valve timing response is slowed down to have smooth transient combustion timing response when the engine operating mode changes. The fueling rate response is kept fast in order to reach the desired load quickly. Details of the input and output constraints are explained in controller structure section. The main objective of the controller is the tracking of the desired output work and combustion timing. The desired combustion timing and output work trajectories are considered as step functions to check the response to a fast system transient.

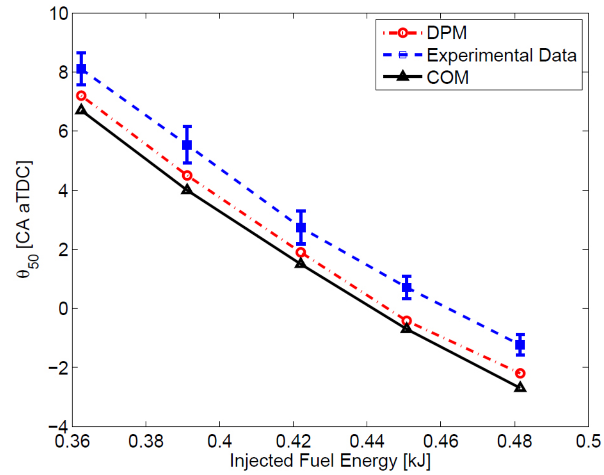

Figure 5. Steady state model validation - NVO=60 Deg CA, ω=817 RPM, P_{int}= 88.3 kPa, T_{int}=80°C and fueling rate is varied at constant airflow rate

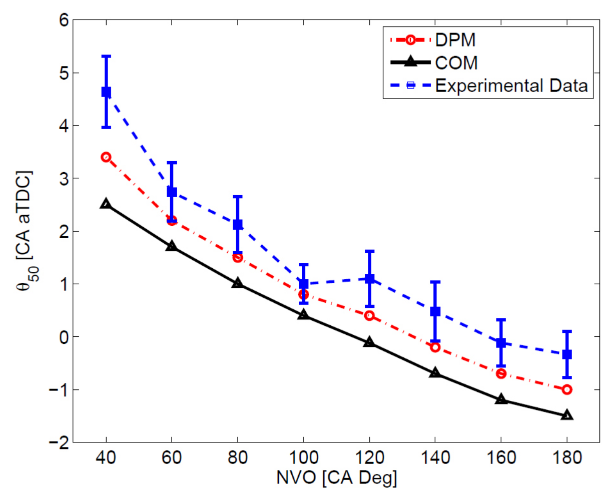

Figure 6. Steady state model validation - Injected Fuel Energy = 0.42 KJ, ω=817 RPM, P_{int}=88.343 kPa, T_{int}=80°C and NVO duration is varied

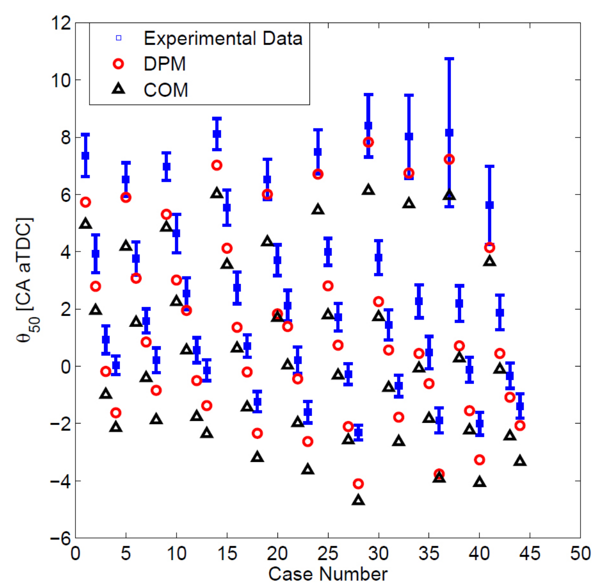

Figure 7. Steady state validation of COM and DPM

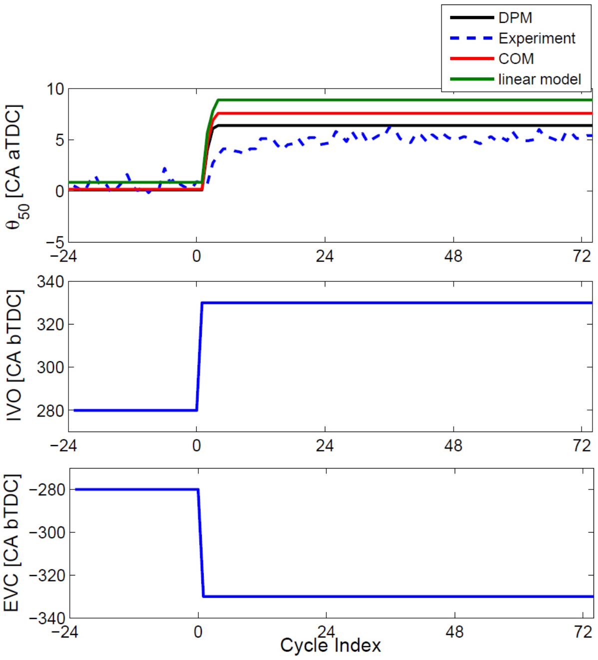

Figure 8. Transient model validation

Controller Structure

The controller is designed based on [56]. The standard state space model, Equation 20, is augmented with an integrator. The augmented model is

$$x(k+1) = A_e x(k) + B_e \Delta u$$
$$y(k) = C_e x(k) \tag{22}$$

where $A_e = \begin{bmatrix} A & 0_n^T \\ CA & 1 \end{bmatrix}$, $B_e = \begin{bmatrix} B \\ CB \end{bmatrix}$ and $C_e = \begin{bmatrix} 0_n & 1 \end{bmatrix}$.

Matrix 0_n has as many columns as matrix A in Equation 20. The augmented model states in Equation 22 are $x(k) = \begin{bmatrix} \Delta x(k) \\ y(k) \end{bmatrix}$ where $\Delta x(k) = x(k) - x(k-1)$ and $x(k)$ are model states from Equation 20.

The control signal and input matrix in Equation 22 are partitioned as:

$$\Delta u(k) = \begin{bmatrix} \Delta u_1(k) & \Delta u_2(k) & \cdots & \Delta u_m(k) \end{bmatrix}$$
$$B_e = \begin{bmatrix} B_1(k) & B_2(k) & \cdots & B_m(k) \end{bmatrix} \tag{23}$$

The controller signal is written based on Laguerre function parameters [56] as:

$$\Delta u_i = L_i(k)^T \eta_i \tag{24}$$

where η_i and $L_i(k)$ are the Laguerre function description of the ith control input and $L_i(k)$ is written as

$$L_i(k)^T = \begin{bmatrix} l_1^i(k) & l_2^i(k) & \ldots & l^i{}_{N_i}(k) \end{bmatrix} \tag{25}$$

and N_i is a scaling factor [56] (here N_i=5). Within this framework, the control horizon concept used in previous studies [10, 23, 47, 49] is eliminated. N_i is used to describe the complexity of the input signal trajectory in conjunction with the Laguerre function pole locations. Larger values for pole locations can be selected to achieve a longer control horizon with a smaller number of N_i in the optimization procedure. The Laguerre function is used to speed up calculations for realtime implementation. For this two input-two output system each input signal is designated to have a Laguerre pole location at 0:5. The prediction of the future states based on the partitioned input matrix is:

$$x(k+m) = A_e^m x(k) + \phi(m)^T \eta \tag{26}$$

with the prediction horizon, m, is chosen to be 10, and η and ϕ are:

$$\eta^T = \begin{bmatrix} \eta_1^T & \eta_2^T & \ldots & \eta_m^T \end{bmatrix} \tag{27}$$

$$\phi(m)^T = \sum_{j=0}^{m-1} A_e^{m-j-1} \begin{bmatrix} B_1 L_1(j)^T \; B_2 L_2(j)^T & \cdots & B_m L_m(j)^T \end{bmatrix} \tag{28}$$

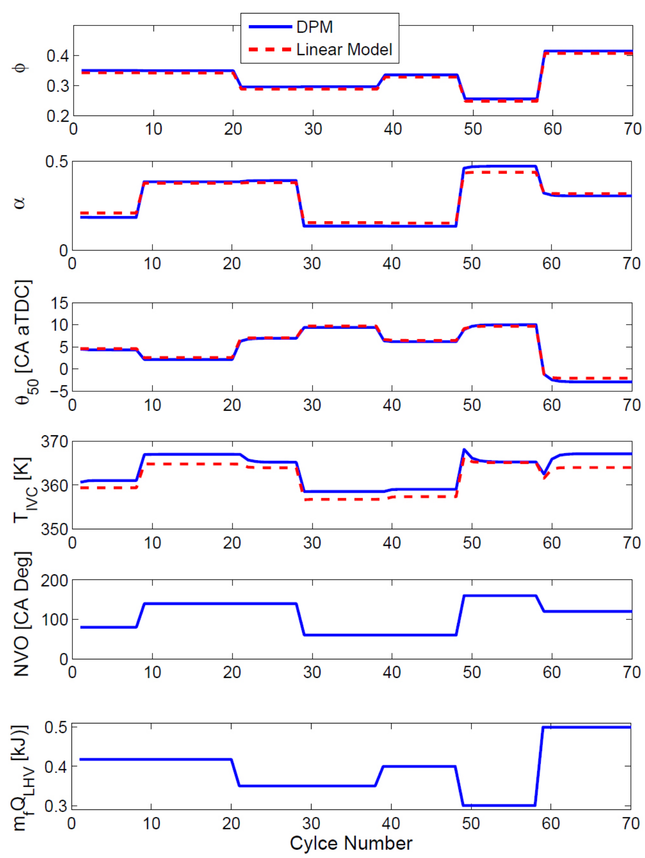

Figure 9. Linear model versus DPM [ω=825 RPM, P_{int}=95 kPa and T_{int}=80°C]

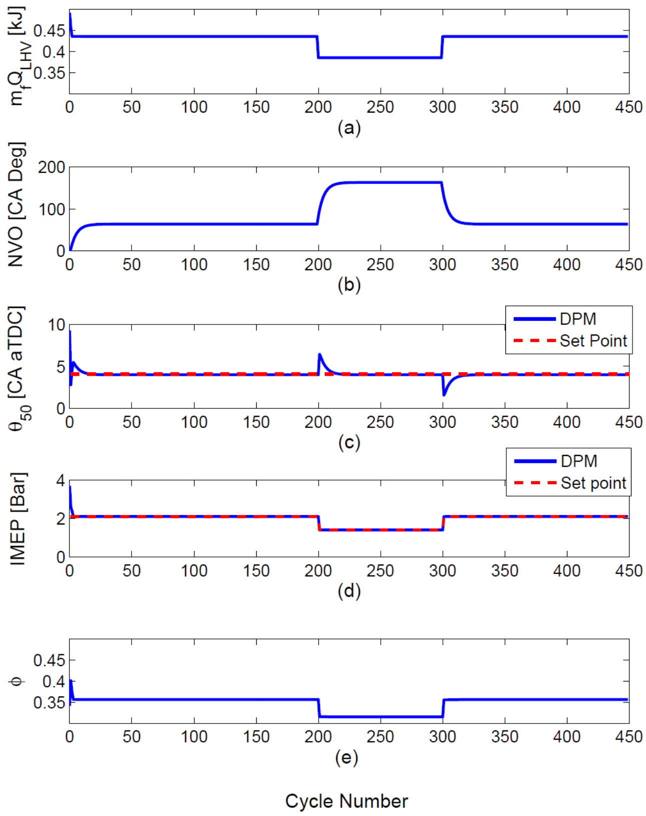

Figure 10. Controller performance (unconstrained): (a) & (b) controller outputs (c) & (d) system outputs (e) fuel equivalence ratio [ω=825 RPM, P_{int}=95 kPa and T_{int}=80°C]

With this approach, predictions of state variables are expressed in terms of the coefficient vector η of the Laguerre function. The cost function is a minimization of the error between the set-point signal and the output signal [56] and is:

$$J = \eta^T \Omega \eta + 2\eta^T \psi x(k) + \sum_{m=1}^{N_p} x(k)^T (A_e^T)^m Q A_e^m x(k) \tag{29}$$

where Ω and ψ are:

$$\Omega = \sum_{m=1}^{m} \phi(m) Q \phi(m)^T + R_L \tag{30}$$

$$\psi = \sum_{m=1}^{m} \phi(m) Q A_e^m \tag{31}$$

with the weighting matrices Q and R_L.

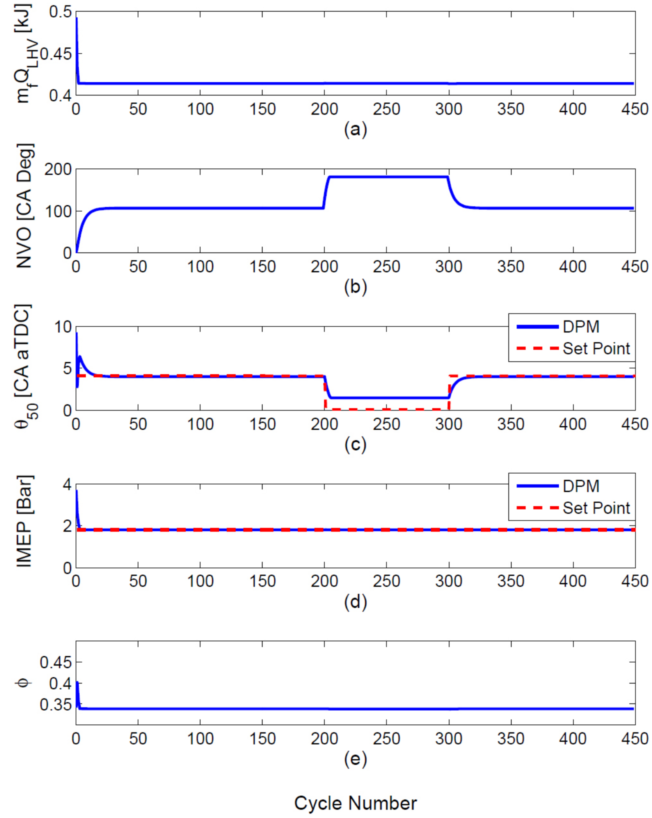

Figure 11. Controller performance (constrained inputs): (a) & (b) controller outputs (c) & (d) system outputs (e) fuel equivalence ratio [ω=825 RPM, P_{int}=95 kPa and T_{int}=80°C] NVO saturation

The optimal solution of cost function without considering constraints is [56]:

$$\eta = -\Omega^{-1} \psi x(k) \tag{32}$$

and the control law is:

$$\Delta u(k) = \begin{pmatrix} L_1(0)^T & 0_2{}^T & \cdots & 0_m{}^T \\ 0_1{}^T & L_2(0)^T & \cdots & 0_m{}^T \\ \vdots & \vdots & \ddots & \vdots \\ 0_1{}^T & 2^T & \cdots & L_m(0)^T \end{pmatrix} \eta \tag{33}$$

where 0_i^T represents a zero block row vector with identical dimension to $L_i(0)^T$. The control variable $\Delta u(k)$ is written in the form of linear state feedback control as:

$$\Delta u(k) = -K_{MPC} x(k) \tag{34}$$

with a controller gain of:

$$K_{MPC} = \begin{pmatrix} L_1(0)^T & 0_2{}^T & \cdots & 0_m{}^T \\ 0_1{}^T & L_2(0)^T & \cdots & 0_m{}^T \\ \vdots & \vdots & \ddots & \vdots \\ 0_1{}^T & 2^T & \cdots & L_m(0)^T \end{pmatrix} \Omega^{-1} \psi \tag{35}$$

The closed loop feedback control is:

$$x(k+1) = (A_e - B_e K_{MPC})\, x(k) \tag{36}$$

To consider constraints on the inputs, outputs and rate of change of input signals the cost function must consider them [56, 63]. The constraints on rate of change of the input signal are:

$$\Delta u_{min} < \begin{pmatrix} L_1(0)^T & 0_2{}^T & \cdots & 0_m{}^T \\ 0_1{}^T & L_2(0)^T & \cdots & 0_m{}^T \\ \vdots & \vdots & \ddots & \vdots \\ 0_1{}^T & 2^T & \cdots & L_m(0)^T \end{pmatrix} \eta < \Delta u_{max} \tag{37}$$

where Δu_{min} and Δu_{max} are the minimum and maximum rate of change of plant input signal respectively. The constraints on the input signals are:

$$u_{min} < \begin{pmatrix} L_1(0)^T & 0_2{}^T & \cdots & 0_m{}^T \\ 0_1{}^T & L_2(0)^T & \cdots & 0_m{}^T \\ \vdots & \vdots & \ddots & \vdots \\ 0_1{}^T & 2^T & \cdots & L_m(0)^T \end{pmatrix} \eta + u(k-1) < u_{max} \tag{38}$$

where u_{min} and u_{max} are the minimum and maximum values of the plant input signal respectively. Finally the output constraints are:

$$y_{min} < CA_e^m x(k) + C_e \phi(m)^T \eta < y_{max} \tag{39}$$

where y_{min} and y_{max} are the minimum and maximum values of the plant output. The minimum and maximum values of the plant input and output signals used are listed in Table 3. The input constraints are hard constraints due to actuator limits while the output constraints are soften by slack variables. Other constraints can be considered by rearranging the COM. For example constraints on the rate of pressure rise or air-fuel ratio have been investigated in [23, 48].

Controller Performance

The controller is tested in simulation using the DPM as the virtual engine. The MPC is tested with constant engine speed, intake manifold pressure and temperature first and then effects of load and speed disturbances are examined. Controller performance, without considering constraints on inputs and outputs, is shown in Figure 10 and both θ_{50} and IMEP closely track the setpoint. Examining the figure closely, at cycle 200 when the desired IMEP is reduced, EVC timing is advanced and NVO duration is increased to trap more residual gas which maintains the combustion timing at 4 Deg CA aTDC.

Table 3. Minimum and maximum values of the input and output signals

	Minimum	Maximum
Injected Fuel Energy [kJ]	0.3	0.5
Injected Fuel Energy Rate [$\frac{kJ}{Cycle}$]	-0.1	0.1
NVO [CA Deg]	0	180
NVO Rate [$\frac{CADeg}{Cycle}$]	-20	20
IMEP [Bar]	0.68	2.5
θ_{50} [CA Deg aTDC]	0	8

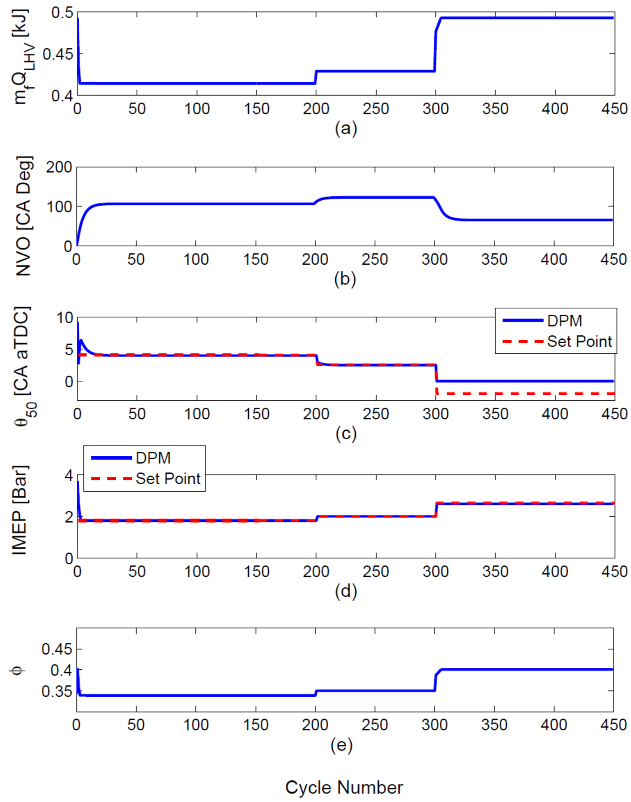

Figure 12. Controller performance (constrained combustion timing): (a) & (b) controller outputs (c) & (d) system outputs (e) fuel equivalence ratio [ω=825 RPM, P_{int}=95 kPa and T_{int}=80°C]

Controller performance considering input constraints is shown in Figure 11. In this case, the desired IMEP is held constant while the desired combustion timing is advanced. To advance the combustion timing, NVO duration is increased by controller to increase the trapped residual gas. At cycle 204, the NVO duration reaches the maximum constraint of 180 Deg CA so the NVO duration saturates at 180 Deg CA. The value of θ_{50} does not track the desired trajectory. This is attributed to NVO saturation after cycle 204 where the controller keeps fueling rate constant to maintain IMEP (load).

The controller performance with an output constraint is shown in Figure 12. The combustion timing lower limit is set to 0 CA Deg after TDC to avoid engine ringing. After cycle 300, the controller does not track the desired combustion trajectory since the desired trajectory is set at 2 CA Deg bTDC. To check the controller performance to a constraint on output work, a maximum limit for IMEP of 2.5 bar based on experiments [30] is set. This limit is based on the engine ringing limit. Thus in Figure 13, when the desired IMEP is increased to 2.8 bar after cycle 300 the controller, maintains the maximum limit of 2.5 bar. In this case, the controller maintains the engine output at the maximum load limit while trying to maintain the combustion timing at 3 CA Deg aTDC. However, the NVO duration reaches the lower limit of 0 CA Deg so the desired combustion timing is not obtained after cycle 300 due to the constraint. The constraints on θ_{50} and output work are sufficient for safe engine operation. The upper and lower bounds are determined from experimental ringing and misfire limits [30].

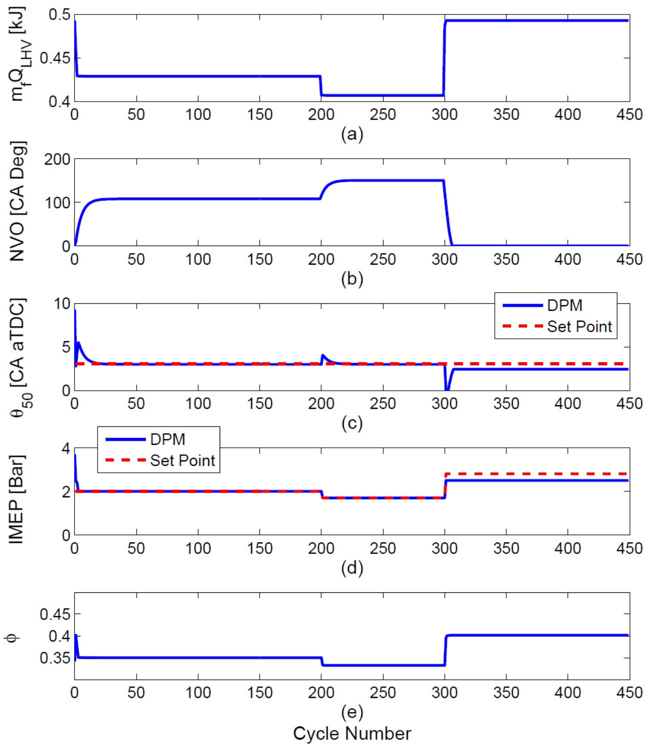

Figure 13. Controller performance (constrained load): (a) & (b) controller outputs (c) & (d) system outputs (e) fuel equivalence ratio [ω=825 RPM, P_{int}=95 kPa and T_{int}=80°C]

The controller performance is tested when both desired combustion timing and load are varied and the results are shown in Figure 14. The controller is able to track both desired combustion timing and load accurately when they are changed simultaneously. Figure 15 shows the controller performance considering the sensor noise effects. The effect of measurement noise on tracking performance of the MPC is studied by adding a Gaussian disturbed noise with standard deviation of 0.7 CAD to the measurement of θ_{50}. The noise level is determined based on observations in [30]. The controller maintains tracking despite the measurement noise in the feedback signal. The controller is also tested with the disturbances of engine load and speed. Figures 16 and 17 show the disturbance rejection properties of the controller for positive and negative disturbance step changes in fuel equivalence ratio and engine speed. The results show that the controller has reasonable disturbance rejection for these cases.

For implementation on the engine an observer is required. When the controller is run in simulation, states like temperature at IVC, θ_{50}, fuel equivalence ratio and residual mole fraction are calculated by DPM and are available to the controller. However, for real time implementation, there is no sensor on the engine to measure those states so an observer is required to predict them. Further constraints, like constraints on the air-fuel ratio and rate of pressure rise can be considered by augmenting the linearized COM model.

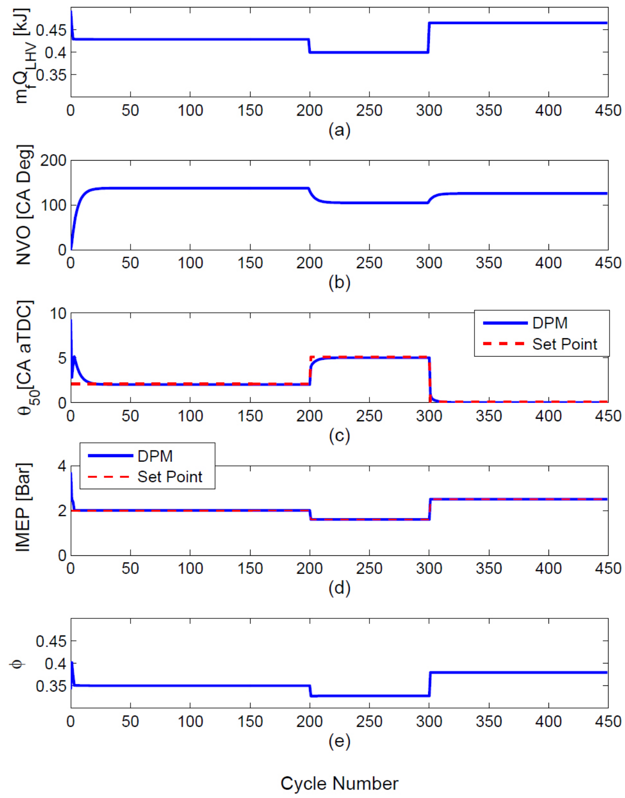

Figure 14. Controller performance (both desired IMEP and θ_{50} are changed at the same time): (a) & (b) controller outputs (c) & (d) system outputs (e) fuel equivalence ratio [ω=825 RPM, P_{int}=95 kPa and T_{int}=80°C]

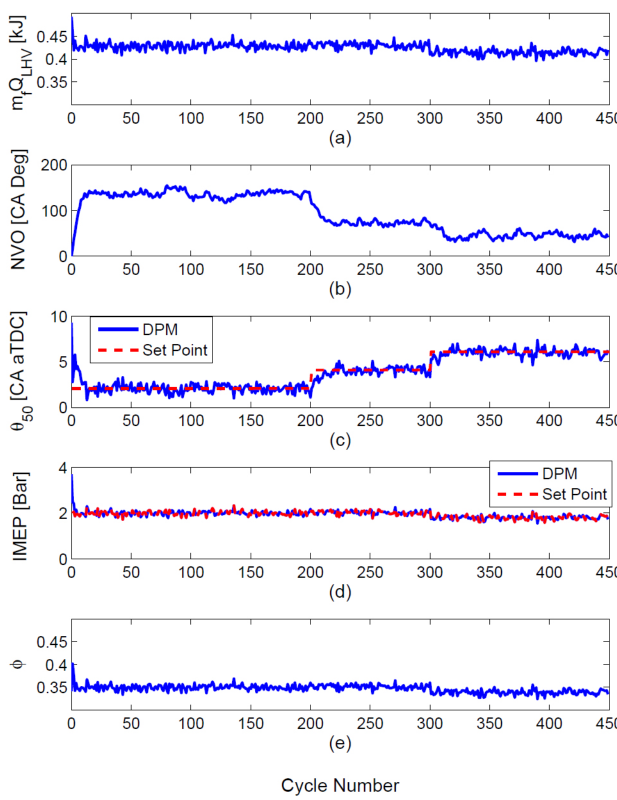

Figure 15. Controller performance considering measurement noise: (a) & (b) controller outputs (c) & (d) system outputs (e) fuel equivalence ratio [ω=825 RPM, P_{int}=95 kPa and T_{int}=80°C]

Conclusions

A 4-state nonlinear control oriented model is developed for cycle by cycle combustion timing and load control. The model is validated against a detailed physical model and experimental data. The nonlinear model shows acceptable accuracy in predicting HCCI combustion timing and load. The model is then linearized around one operating point and the 5-state linearized model is used to design a discrete MPC using Laguerre functions. The MPC shows good performance for combustion timing and load control in HCCI engine using a detailed physical model for the engine. The controller performs well in maintaining a desirable engine operation during load and engine speed disturbances. NVO duration and fueling rate are used as main actuators for combustion timing and load control. Simulation results show that the MPC controller satisfies all the desired objectives, and can track the desired load and combustion timing trajectories while considering actuator restrictions and output constraints. Both the nonlinear control oriented model and controller have a simple structure and that is amenable to being parameterized for other fuels like bio-fuels since the DPM is physical based.

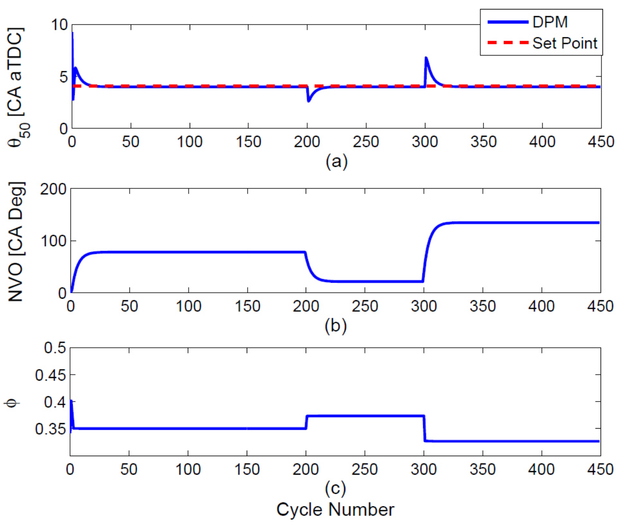

Figure 16. Disturbance rejection: Engine load (a) θ_{50} (b) Controller Input and (c) Disturbance [ω=825 RPM, P_{int}=95 kPa and T_{int}=80°C]

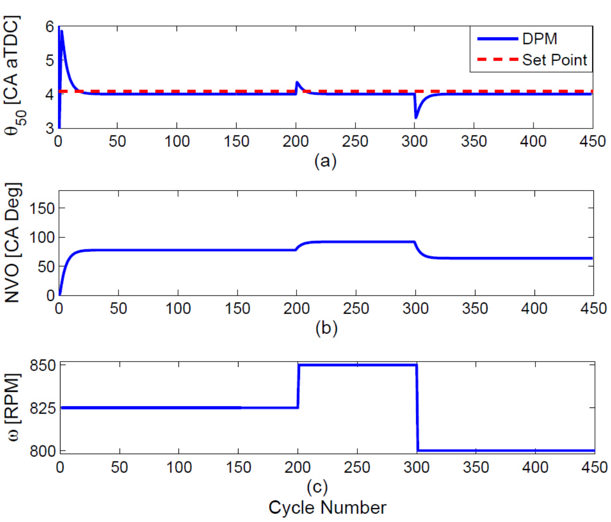

Figure 17. Disturbance rejection: Engine speed (a) θ_{50} (b) Controller Input and (c) Disturbance [IMEP=1.9 Bar, P_{int}=95 kPa and T_{int}=80°C]

Definitions/Abbreviations

DPM - Detailed Physical Model

COM - Control Oriented Model

SI - Spark Ignition

CO - Carbon Monoxide

HC - Hydrocarbons

NO_X - Nitric Oxide

IVC - Intake Valve Closing

IVO - Intake Valve Opening

EVC - Exhaust Valve Closing

EVO - Exhaust Valve Opening

HCCI - Homogeneous Charge Compression Ignition

NVO - Negative Valve Overlap

TDC - Top Dead Center

VVT - Variable Valve Timing

CA Deg - Crank Angle Degree

ON - Octane Number

PID - Proportional Integral-Derivative

LQG - Linear Quadratic Gaussian

θ_{50} - Crank angle of fifty percent fuel mass fraction burned

MPC - Model Predictive Control

DSMC - Discrete Sliding Mode Controller

PRF - Primary Reference Fuel

SOC - Start Of Combustion

LHV - Lower Heating Value

T - Temperature

P - Pressure

RES - Residual

exh - exhaust

N_2 - Nitrogen

O_2 - Oxygen

H_2O - Water

C_7H_{16} - n-heptane

CO_2 - Carbon Dioxide

C_p - Specific heat at constant pressure

BC - Before Combustion

AC - After Combustion

V - in-cylinder Volume

ϕ - fuel equivalence ratio

α - residual mole fraction

m_{fuel} - mass of injected fuel

$\Delta\theta$ - combustion duration

IMEP - Indicated Mean Effective Pressure

k - cycle number

ω - Engine speed

int - intake

EGR - Exhaust Gas Recirculation

aTDC - after Top Dead Center

bTDC - before Top Dead Center

RPM - Revolutions Per Minute

kJ - kilojoules

References

1. Zhao H.. *HCCI and CAI engines for the automotive industry.* CRC Press, 2006. ISBN 9781845691288.
2. Westbrook C. K., Mizobuchi Y., Poinsot T. J., Smith P. J., and Warnatz J.. Computational combustion. *Proceedings of the Combustion Institute*, 30(1):125-157, 2005. ISSN 1540-7489.
3. Yao M., Zheng Z., and Liu H.. Progress and recent trends in homogeneous charge compression ignition (HCCI) engines. *Progress in Energy and Combustion Science*, 35(5):398-437, 2009. ISSN 0360-1285.
4. Killingsworth N. J., Aceves S. M., Flowers D. L., Espinosa-Loza F., and Krstic M.. HCCI engine combustion-timing control: Optimizing gains and fuel consumption via extremum seeking. *Control Systems Technology, IEEE Transactions on*, 17(6): 1350-1361, Nov 2009. ISSN 1063-6536.
5. Najt, P. and Foster, D., "Compression-Ignited Homogeneous Charge Combustion," SAE Technical Paper 830264, 1983, doi:10.4271/830264.
6. Chun-hua Z., Jiang-ru P., Juan-juan T., and Jing L.. Effects of intake temperature and excessive air coefficient on combustion characteristics and emissions of HCCI combustion. *Procedia Environmental Sciences*, 11, Part C(0):1119-1127, 2011. ISSN 1878-0296. 2011 2nd International Conference on Challenges in Environmental Science and Computer Engineering (CESCE 2011), doi:10.1016/j.proenv.2011.12.169.
7. Mahrous A.-F., Potrzebowski A., Wyszynski M., Xu H., Tsolakis A., and Luszcz P.. A modelling study into the effects of variable valve timing on the gas exchange process and performance of a 4-valve DI homogeneous charge compression ignition (HCCI) engine. *Energy Conversion and Management*, 50(2), 2009, doi:10.1016/j.enconman.2008.09.018. ISSN 0196-8904.
8. Xie H., Li L., Chen T., and Zhao H.. Investigation on gasoline homogeneous charge compression ignition (HCCI) combustion implemented by residual gas trapping combined with intake preheating through waste heat recovery. *Energy Conversion and Management*, 86(0):8-19, 2014. ISSN 0196-8904. doi:10.1016/j.enconman.2014.05.022.
9. Zhou, N., Xie, H., Li, N., Chen, T. et al., "Study on Layered Close Loop Control of 4-Stroke Gasoline HCCI Engine Equipped with 4VVAS," SAE Technical Paper 2008-01-0791, 2008, doi:10.4271/2008-01-0791.
10. Bengtsson J., Strandh P., Johansson R., Tunestål P., and Johansson B.. Model predictive control of Homogeneous Charge Compression Ignition (HCCI) engine dynamics. In *Computer Aided Control System Design, 2006 IEEE International Conference on Control Applications, 2006 IEEE International Symposium on Intelligent Control, 2006 IEEE*, pages 1675-1680, Oct 2006. doi:10.1109/CACSD-CCA-ISIC.2006.4776893.
11. Shaver G., Roelle M., and Gerdes J.. Decoupled control of combustion timing and work output in residual- affected HCCI engines. In *Proceedings of the 2005 American Control Conference*, pages 3871-3876 vol. 6, June 2005. doi:10.1109/ACC.2005.1470578.
12. Ebrahimiand K., Koch C. R., HCCI combustion timing control with variable valve timing. In *Proceedings of the 2013 American Control Conference*, pages 4429-4434, June 2013. doi:10.1109/ACC.2013.6580522.
13. Rausen D. J., Stefanopoulou A. G., Kang J. M., Eng J. A., and Kuo T. W.. A mean-value model for control of homogeneous charge compression ignition (HCCI) engines. In *Proceedings of the 2004 American Control Conference*, volume 1, pages 125-131, 30 June-2 July 2004. ISSN 0743-1619.
14. Kang J. M. and Druzhinina M.. HCCI engine control strategy with external EGR. In *Proceedings of the 2010 American Control Conference*, pages 3783-3790, June 2010. doi:10.1109/ACC.2010.5531558.
15. Fathi M., Saray R. K., and Checkel M. D.. The influence of Exhaust Gas Recirculation (EGR) on combustion and emissions of n-heptane/natural gas fueled Homogeneous Charge Compression Ignition (HCCI) engines. *Applied Energy*, 88(12): 4719-4724, 2011. ISSN 0306-2619. doi:10.1016/j.apenergy.2011.06.017.
16. Maurya, R. and Agarwal, A., "Experimental Investigation of Close-Loop Control of HCCI Engine Using Dual Fuel Approach," SAE Technical Paper 2013-01-1675, 2013, doi:10.4271/2013-01-1675.
17. Audet, A. and Koch, C., "Actuator Comparison for Closed Loop Control of HCCIC Combustion Timing," SAE Technical Paper 2009-01-1135, 2009, doi:10.4271/2009-01-1135.
18. Bengtsson J., Strandh F., Johansson R., Tunestål P., and Johansson B.. Control of homogeneous charge compression ignition (HCCI) engine dynamics. In *Proceedings of the 2004 American Control Conference*, volume 5, pages 4048-4053 vol.5, June 2004. ISSN 0743-1619.
19. Bidarvatan M., Shahbakhti M., Jazayeri S., and Koch C.. Cycle-to-cycle modeling and sliding mode control of blended-fuel HCCI engine. *Control Engineering Practice*, 24(0):79-91, 2014. doi:10.1016/j.conengprac.2013.11.008.
20. Haraldsson, G., Tunestal, P., Johansson, B., and Hyvönen, J., "HCCI Combustion Phasing with Closed-Loop Combustion Control Using Variable Compression Ratio in a Multi Cylinder Engine," SAE Technical Paper 2003-01-1830, 2003, doi:10.4271/2003-01-1830.
21. Haraldsson, G., Tunestal, P., Johansson, B., and Hyvönen, J., "HCCI Combustion Phasing in a Multi Cylinder Engine Using Variable Compression Ratio," SAE Technical Paper 2002-01-2858, 2002, doi:10.4271/2002-01-2858.
22. Yun, H., Wermuth, N., and Najt, P., "Development of Robust Gasoline HCCI Idle Operation Using Multiple Injection and Multiple Ignition (MIMI) Strategy," SAE Technical Paper 2009-01-0499, 2009, doi:10.4271/2009-01-0499.
23. Ravi N., Liao H.-H., Jungkunz A. F., Widd A., and Gerdes J. C.. Model predictive control of HCCI using variable valve actuation and fuel injection. *Control Engineering Practice*, 20(4): 421-

430, 2012. ISSN 0967-0661. Special Section: IFAC Symposium on Advanced Control of Chemical Processes - ADCHEM 2009, doi:10.1016/j.conengprac.2011.12.002.

24. Christensen, M. and Johansson, B., "Homogeneous Charge Compression Ignition with Water Injection," SAE Technical Paper 1999-01-0182, 1999, doi:10.4271/1999-01-0182.
25. Iwashiro, Y., Tsurushima, T., Nishijima, Y., Asaumi, Y. et al., "Fuel Consumption Improvement and Operation Range Expansion in HCCI by Direct Water Injection," SAE Technical Paper 2002-01-0105, 2002, doi:10.4271/2002-01-0105.
26. Fang Q., Fang J., Zhuang J., and Huang Z.. Influences of pilot injection and exhaust gas recirculation (EGR) on combustion and emissions in a HCCI-DI combustion engine. *Applied Thermal Engineering*, 48(0):97-104, 2012. ISSN 1359-4311.
27. Mahrous, A., Potrzebowski, A., Wyszynski, M., Xu, H. et al., "A 1D Analysis into the Effect of Variable Valve Timing on HCCI Engine Parameters," SAE Technical Paper 2008-01-2459, 2008, doi:10.4271/2008-01-2459.
28. Kang, J., Chang, C., and Kuo, T., "Sufficient Condition on Valve Timing for Robust Load Transients in HCCI Engines," SAE Technical Paper 2010-01-1243, 2010, doi:10.4271/2010-01-1243.
29. Ebrahimi K., Schramm A., and Koch C. R.. Effects of asymmetric valve timing with constant NVO duration on HCCI engine combustion characteristics. In *Combustion Institute/Canadian Section (CI/CS) Spring Technical Meeting, Windsor, ON*, 2014.
30. Schramm A.. Effects of negative valve overlap on HCCI combustion and its use in the control of HCCI combustion timing. Master's thesis, University of Alberta, 2014.
31. Ebrahimi K., Schramm A., and Koch C. R.. Feed-forward/feedback control of HCCI combustion timing. In *Proceedings of the 2014 American Control Conference, Portland, USA*, page 6, 2014. doi:10.1109/ACC.2014.6858910.
32. Ebrahimi, K., Koch, C., and Schramm, A., "A Control Oriented Model with Variable Valve Timing for HCCI Combustion Timing Control," SAE Technical Paper 2013-01-0588, 2013, doi:10.4271/2013-01-0588.
33. Pfeiffer R., Haraldsson G., Olsson J. O., Tunestål P., Johansson R., and Johansson B.. System identification and LQG control of variable-compression HCCI engine dynamics. In *Proceedings of the 2004 IEEE International Conference*, volume 2, pages 1442-1447 Vol.2, Sept 2004. doi:10.1109/CCA.2004.1387578.
34. Shaver G., Gerdes J., and Roelle M.. Physics-based closed-loop control of phasing, peak pressure and work output in HCCI engines utilizing variable valve actuation. In *Proceedings of the 2004 American Control Conference*, volume 1, pages 150-155 vol.1, June 2004. ISSN 0743-1619.
35. Olsson, J., Tunestal, P., and Johansson, B., "Closed-Loop Control of an HCCI Engine," SAE Technical Paper 2001-01-1031, 2001, doi:10.4271/2001-01-1031.
36. Haraldsson, G., Tunestal, P., Johansson, B., and Hyvönen, J., "HCCI Closed-Loop Combustion Control Using Fast Thermal Management," SAE Technical Paper 2004-01-0943, 2004, doi:10.4271/2004-01-0943.
37. Lee D., Stefanopoulou A., Makkapati S., and Jankovic M.. Modeling and control of a heated air intake homogeneous charge compression ignition (HCCI) engine. In *Proceedings of the 2010 American Control Conference*, pages 3817-3823, June 2010. doi: 10.1109/ACC.2010.5531442.
38. Rausen D., Stefanopoulou A., Kang J. M., Eng J., and Kuo T.. A mean-value model for control of homogeneous charge compression ignition (HCCI) engines. *Journal of Dynamic Systems, Measurement, and Control*, (3):355, 2005. ISSN 0022-0434.
39. Strandh, P., Bengtsson, J., Johansson, R., Tunestål, P. et al., "Cycle-to-Cycle Control of a Dual-Fuel HCCI Engine," SAE Technical Paper 2004-01-0941, 2004, doi:10.4271/2004-01-0941.
40. Shaver G., Roelle M., and Gerdes J.. A two-input two-output control model of HCCI engines. In *Proceedings of the 2006 American Control Conference*, June 2006. doi:10.1109/ACC.2006.1655401.
41. Souder J. S.. *Closed-Loop Control of a Multi-Cylinder HCCI Engine.* PhD thesis, University of California, Berkeley, 2004.
42. Ravi N., Roelle M., Liao H. H., Jungkunz A., Chang C. F., Park S., and Gerdes J.. Model-Based Control of HCCI Engines Using Exhaust Recompression. *IEEE Transactions on Control Systems Technology*, 18(6):1289-1302, Nov 2010.
43. Franz, J., Schwarz, F., Guenthner, M., Reissing, J. et al., "Closed Loop Control of an HCCI Multi-Cylinder Engine and Corresponding Adaptation Strategies," SAE Technical Paper 2009-24-0079, 2009, doi:10.4271/2009-24-0079.
44. Agrell, F., Ängström, H., Eriksson, B., Wikander, J. et al., "Integrated Simulation and Engine Test of Closed Loop HCCI Control by Aid of Variable Valve Timings," SAE Technical Paper 2003-01-0748, 2003, doi:10.4271/2003-01-0748.
45. Bidarvatan, M. and Shahbakhti, M., "Two-Input Two- Output Control of Blended Fuel HCCI Engines," SAE Technical Paper 2013-01-1663, 2013, doi:10.4271/2013-01-1663.
46. Bidarvatan M. and Shahbakhti M.. Integrated HCCI engine control based on a performance index. *Journal of Engineering for Gas Turbines and Power*, (10): 101601,. ISSN 0742-4795, doi:10.1115/1.4027279.
47. Erlien S. M., Jungkunz A. F., and Gerdes J. C.. Multi-Cylinder HCCI Control With Cam Phaser Variable Valve Actuation Using Model Predictive Control. In *Proceedings of the 2012 ASME Dynamic Systems and Control Conference*, volume 2, pages 823-832, 2013. doi:10.1115/DSCC2012-M0VIC2012-8585.
48. Bengtsson, J., Strandh, P., Johansson, R., Tunestål, P. et al., "Multi-Output Control of a Heavy Duty HCCI Engine Using Variable Valve Actuation and Model Predictive Control," SAE Technical Paper 2006-01-0873, 2006, doi:10.4271/2006-01-0873.
49. Li, D. and Wang, D., "Multivariable Control of Residual-Affected HCCI Engines Based on Model Predictive Control," SAE Technical Paper 2013-01-2511, 2013, doi:10.4271/2013-01-2511.

50. Shaver G. M., Gerdes J. C., Roelle M. J., Catton P. A., and Christopher F. E.. Dynamic modeling of residual-affected homogeneous charge compression ignition engines with variable valve actuation. *Journal of Dynamics System, Measurement, and Control*, 127:374-381, 2005. doi:10.1115/1.1979511.
51. Swan, K., Shahbakhti, M., and Koch, C., "Predicting Start of Combustion Using a Modified Knock Integral Method for an HCCI Engine," SAE Technical Paper 2006-01-1086, 2006, doi:10.4271/2006-01-1086.
52. Shahbakhti, M., Lupul, R., and Koch, C., "Predicting HCCI Auto-Ignition Timing by Extending a Modified Knock-Integral Method," SAE Technical Paper 2007-01-0222, 2007, doi:10.4271/2007-01-0222.
53. Millet, J., Maroteaux, F., and Ravet, F., "Modeling of HCCI Combustion by One Step Reaction Function: In View of Assisting the Optimization of Engine Management System," SAE Technical Paper 2007-24-0033, 2007, doi:10.4271/2007-24-0033.
54. https://www-pls.llnl.gov/.
55. https://www.erc.wisc.edu/chemicalreaction.php.
56. Wang L.. *Model predictive control system design and implementation using MATLAB*. Advances in industrial control. London : Springer, c2009., 2009. ISBN 1848823312.
57. Shaver G. M., Gerdes J. C., Jane P., Catton P. A., and Edwards C. F.. Modeling for control of HCCI engines. *Proceedings of the American Control Conference*, page 749754, 2003, doi:10.1109/ACC.2003.1239111.
58. Bettis J. B.. Thermodynamic based modeling for nonlinear control of combustion phasing in HCCI engines. Master's thesis, Missouri University of Science and Technology, 2010.
59. Heywood J. B.. *Internal combustion engine fundamentals*. New York : McGraw-Hill, c1988., 1988. ISBN 007028637X.
60. Shahbahkti M.. *Modeling and Experimental Study of an HCCI Engine for Combustion Timing Control*. PhD thesis, University of Alberta, 2009.
61. Guzzella L., Koch C. R., and Scherer M.. USA 6212467: Electronic Engine Control System, USA Patent, 2001.
62. Babajimopoulos, A., Assanis, D., and Fiveland, S., "An Approach for Modeling the Effects of Gas Exchange Processes on HCCI Combustion and Its Application in Evaluating Variable Valve Timing Control Strategies," SAE Technical Paper 2002-01-2829, 2002, doi:10.4271/2002-01-2829.
63. Tøndel P., Johansen T. A., and Bemporad A.. An algorithm for multi-parametric quadratic programming and explicit MPC solutions. *Automatica*, 39(3):489-497, 2003. ISSN 0005-1098. doi:10.1016/S0005-1098(02)00250-9.

The Engineering Meetings Board has approved this paper for publication. It has successfully completed SAE's peer review process under the supervision of the session organizer. The process requires a minimum of three (3) reviews by industry experts.

ISSN 0148-7191

http://papers.sae.org/2015-01-0822